Improved 3-D Analytical Model for Axial-Flux Eddy-Current Couplings with Curvature Effects

Thierry Lubin, Abderrezak Rezzoug

Improved 3-D Analytical Model for Axial-Flux Eddy-Current Couplings with Curvature Effects

Thierry Lubin and Abderrezak Rezzoug

Université de Lorraine, Groupe de Recherche en Electrotechnique et Electronique de Nancy, GREEN, F-54500 Vandœuvre-lès-Nancy, France

An improved three-dimensional analytical model for axial-flux permanent-magnet eddy-current couplings is presented in this paper. As the problem is solved in a 3-D cylindrical coordinate system, the proposed model directly takes into account the radial edge effects and the curvature effects on the torque prediction without the need of any correction factor. It is shown that the new analytical model is very accurate, even for the geometries where the curvature effects are very pronounced. Another advantage of the proposed model is the great reduction of computation time compared to 3-D finite elements simulations and an easier adaptation for parametric studies and optimization.

***Index Terms*—Analytical modeling, curvature effects, eddy-current, magnetic coupling, three-dimensional, torque.**

I. Introduction

Analytical models available in the literature for the analysis of axial-field eddy-current magnetic couplings are usually based on 2-D approximations. The problem is solved in a Cartesian coordinate system under the mean radius development hypothesis and by considering an infinite depth for the magnets and the conducting region. The induced currents are then obtained by solving a 2-D diffusion equation [1]-[7] or by using the magnetic equivalent circuit (MEC) method [8]-[10]. The 3-D radial edge effects, which cannot be neglected for such devices, are taken into account by using the well-known Russel and Norsworthy's correction factor [11]. However, it has been shown that this correction factor is not always accurate [5], [6]. Its precision greatly depends on the slip speed and on the coupling geometry: radial depth and pole pitch values.

Unfortunately, the shift to a 3-D analytical model is not an easy task because of the induced currents determination in the moving conducting region which leads to mathematical difficulties. It is then not surprising to find very few papers about it in the literature. However, it is the only way to directly take into account the radial edge effects without the need of a correction factor. Some mathematical difficulties can be overcome by solving this problem in 3-D Cartesian coordinates. The 3-D cylindrical topology shown in Fig. 1 can be reduced to an equivalent 3-D linear structure by using the mean radius assumption [12]-[14]. Such model allows taking into account the radial edge effects and leads to accurate calculation of the torque and the axial force as long as the curvature effects can be neglected.

Compared to our previous work [14] where the curvature effects was neglected, the objective of this paper is to develop an improved 3-D analytical model which is able to consider both the edge effects in the radial direction and the curvature effects. This is a very important issue if the analytical model is intended to be used in a design optimization procedure where the geometrical parameters can vary significantly.

As the axial-flux magnetic coupling presents natural cylindrical boundaries (Fig .1), the problem will be directly solved in a 3-D cylindrical coordinate system (r, θ, z) thanks to the method of separation of variables. A magnetic scalar formulation will be used in the nonconducting regions (magnets and airgap) whereas a current density formulation will be used in the conducting regions (copper and back-iron). Compared to previous studies where a second-order potential formulation was used in the conducting regions [17]-[20], a direct formulation in terms of current density appears as a simplest way to solve analytically this 3-D eddy-current problem. In the knowledge of the authors, no 3-D analytical method, similar to that presented here, was found in the literature.

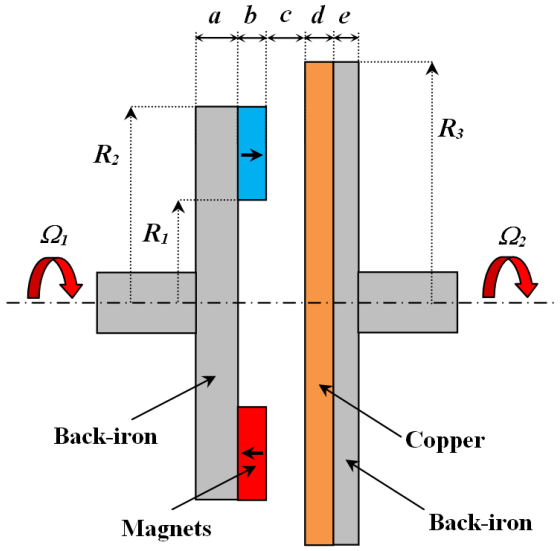

Fig. 1. Cross section of the studied axial-flux permanent magnet eddy-current coupling.

Manuscript received April 9, 2017;
Digital Object Identifier (inserted by IEEE).

From the field solution, the transmitted torque is derived by using the Maxwell stress tensor. The contribution of the torque due to the induced currents in the back-iron (copper side) is also taken into account. The results obtained here are compared with those numerically calculated with a 3-D finite element method, on one hand, and with those previously obtained by the authors thanks to a simplified Cartesian model [14] on the other hand. It is shown that the new analytical model is very accurate, even for the geometries where the curvature effects are very pronounced. Another advantage of the proposed analytical model is the great reduction of computation time compared to the one required for 3-D FE simulations.

II. Problem Description and Assumptions

A. Geometry of the Studied Magnetic Coupling

Fig. 1 shows the cross-section of the studied axial-flux eddy-current coupling. It consists of two movers separated by a small air-gap. The first one is composed of sector shaped rare-earth permanent magnets (PMs) glued to the back-iron. The PMs are magnetized in the axial direction and regularly distributed to obtain alternately north and south poles. The second one is composed of a conducting plate, usually made of copper, screwed to the back-iron. As is well known, the torque-speed characteristic of such device is related to the induced currents in the conducting regions. The value and the distribution of the induced currents depend among other things on the slip speed $\Omega = \Omega_1 - \Omega_2$ where Ω_1 and Ω_2 are respectively the absolute angular speeds of the primary and the secondary movers (Fig. 1).

The geometrical parameters of the studied coupling are given in Fig. 1. We can note that the radius of the copper plate R_3 is chosen significantly greater than R_2. In so doing, the return paths of the induced current are mainly located outside the useful area that corresponds to the magnet depth $(R_2 - R_1)$ and the performances of the magnetic coupling are greatly improved [10], [14].

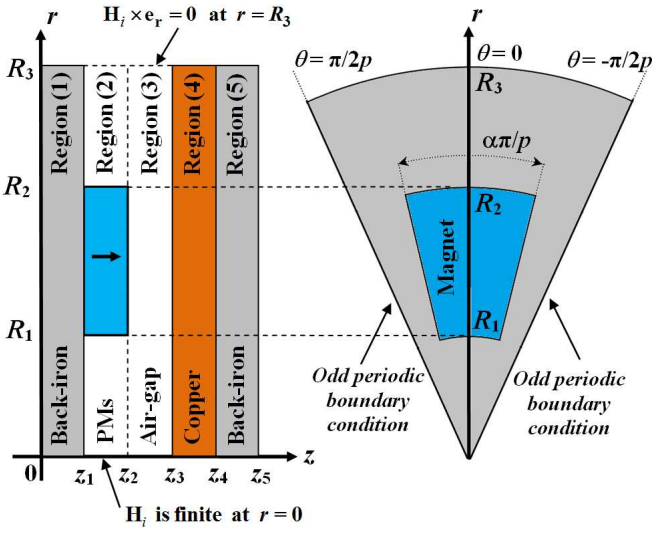

Fig. 2. Five-layer field model of the studied magnetic coupling in the r-z and r-θ planes for one pole-pitch.

B. Field Problem and Assumptions

As shown in Fig. 2, the whole domain of the field problem is divided into five identical wedge-shaped cylindrical regions: the back-iron (region 1), the PMs (region 2), the air-gap (region 3), the copper plate (region 4), and the back-iron of the copper side (region 5). Except their angular phase shift, the PMs and the eddy-current distributions are the same, so the magnetic problem presents an odd periodicity in the θ-direction. The whole domain shown in Fig. 2 is then limited by the planes $\theta = -\pi/2p$ and $\theta = \pi/2p$ where p is the pole-pairs number. In order to simplify the solution of this boundary value problem, it is important to note that the radius of the back-iron of region 1 has been extended to R_3.

To analytically solve this 3-D problem, we suppose a linear behavior of all material media in Fig. 2. The air-gap, the PMs, and the copper plate have the same permeability μ_0 (vacuum permeability) whereas the relative permeability of the back-iron is μ_{rb} (regions 1 and 5). The electrical conductivity of the copper σ_c (region 4) and of its back-iron σ_b (region 5) is considered as constant. Since there are no relative motion between the PMs and the back-iron of region 1, its conductivity has not to be considered. Here, we consider only the steady state operation. The slip speed Ω is considered as a constant term.

In order to facilitate the analytical treatment of this 3-D eddy-current problem, the frame of reference is fixed to the copper plate and its back-iron (regions 4 and 5). In so doing, there will be no speed term in the partial differential equations for the conducting regions. Therefore, for an observer placed in the copper plate, the PMs and its back-iron move with the angular slip speed Ω. The PMs region is then seen as a travelling magnetic wave with a residual magnetization $\mathbf{M}$ which depends on the r-θ spatial coordinates (Fig. 3) and on the time variable t. As the PMs are axially magnetized and the magnetization distribution is $2\pi/p$ periodic in the θ-direction, it can be written as follows with a complex notation:

$$\mathbf{M} = M_z(r,\theta,t)\mathbf{e_z} \tag{1}$$

with

$$M_z(r,\theta,t) = \Re\left\{\sum_{n=1}^{\infty} M_n(r)\, e^{jnp(\theta-\Omega t)}\right\} \tag{2}$$

where $\mathbf{e_z}$ is the unit vector in the z-direction, n is an odd integer, p is the number of pole-pairs, $\Re$ denotes the real part of a complex number and $j = \sqrt{-1}$. The mathematical expression of $M_n(r)$, which depends on the magnetization distribution as shown in Fig. 3, will be developed in the next section. In accordance with the source term (2) and reminding that this problem is $2\pi/p$ periodic in each region, the solution of field quantities will take the following general form

$$X(r,\theta,z,t) = \Re\left\{\sum_{n=1}^{\infty} \overline{X}_n(r,z)\, e^{jnp(\theta-\Omega t)}\right\} \tag{3}$$

where X can denote a magnetic scalar potential for the non-conducting regions 1, 2, and 3, or a component of the current density for the conducting regions 4 and 5. Expression of $X(r,\theta,z,t)$ for each region is developed in the next section.

III. Three Dimensional Analytical Model in Cylindrical Coordinates

A. Boundary Conditions

Fig. 2 summarizes the boundary conditions to be applied for each region (i = 1, 2, 3, 4 and 5) of the studied problem. As indicated previously, the fields apply on two opposite sides (at $\theta = \pm\pi/2p$) is anti-periodic and must check

$$\mathbf{H}_i(r,\pi/2p,z,t) = -\mathbf{H}_i(r,-\pi/2p,z,t) \tag{4}$$

where $\mathbf{H_i}$ is the magnetic field strength in region i.

Boundary conditions are also required in the radial direction to solve this problem. The studied domain is then truncated by an artificial boundary at $r = R_3$. We impose for each region a perfect magnetic boundary condition on the plane at $r = R_3$. Moreover we consider that the magnetic field remains finite at $r = 0$.

$$\mathbf{H}_i \times \mathbf{e}_r = 0 \quad \text{at} \quad r = R_3 \tag{5}$$

$$\mathbf{H}_i \text{ is finite at } r = 0 \tag{6}$$

where $\mathbf{e_r}$ is the unit vector in the r-direction.

It is important to note that for regions 4 and 5, the boundary condition (5) corresponds to a zero value for the radial component of the induced current at $r = R_3$.

As shown in Fig. 2, the field problem is also limited in the z-direction by two boundaries positioned at $z = 0$ and $z = z_5$. On these planes, we impose that no flux line leak out the iron-yoke, which corresponds to fix a flux-parallel boundary condition for regions 1 and 5

$$\mathbf{B}_1 \cdot \mathbf{e_z} = 0 \quad \text{at} \quad z = 0 \tag{7}$$

$$\mathbf{B}_5 \cdot \mathbf{e_z} = 0 \quad \text{at} \quad z = z_5 \tag{8}$$

where $\mathbf{B_1}$ and $\mathbf{B_5}$ are the flux density in region 1 and 5, respectively.

B. Magnetic Field in the Nonconducting Regions

For the nonconducting regions (i = 1, 2, 3), the magnetic field is based on the magnetostatic Maxwell's equations

$$\nabla \cdot \mathbf{B}_i = 0 \qquad \nabla \times \mathbf{H}_i = 0 \tag{9}$$

From (9), the magnetic field strength can be written in terms of a magnetic scalar potential Φ_i, which is defined as

$$\mathbf{H}_i = -\nabla \Phi_i \tag{10}$$

For the permanent magnets, we consider a linear characteristic with a relative permeability near unity (NdFeB magnets) such as

$$\mathbf{B}_i = \mu_0 \mathbf{H}_i + \mu_0 \mathbf{M}_i \qquad (M_i \neq 0 \quad \text{for} \quad i = 2) \tag{11}$$

where $\mathbf{M_i}$ is the remanent magnetization vector defined in (1). Equations (9), (10) and (11) are combined to give

$$\nabla^2 \Phi_i = \nabla \cdot \mathbf{M}_i \tag{12}$$

As indicated in (1), the magnetization vector presents only one z-independent component in the z-direction. The Poisson equation (12) is then simplified to the Laplace equation (13) for all nonconducting regions, which can be written in cylindrical coordinates as

$$\frac{\partial^2 \Phi_i}{\partial r^2} + \frac{1}{r}\frac{\partial \Phi_i}{\partial r} + \frac{1}{r^2}\frac{\partial^2 \Phi_i}{\partial \theta^2} + \frac{\partial^2 \Phi_i}{\partial z^2} = 0 \quad \text{for} \quad i = 1,2,3 \tag{13}$$

The boundary conditions given in (4)-(6) can be re-written in terms of magnetic scalar potential as follows

$$\begin{aligned} &\Phi_i(r,-\pi/2p,z,t) = -\Phi_i(r,\pi/2p,z,t) \\ &\Phi_i(R_3,\theta,z,t) = 0 \\ &\Phi_i(r,\theta,z,t) \text{ is finite at } r = 0 \end{aligned} \tag{14}$$

By using the method of separation of variables, we obtain the general solution of the boundary problem (13)-(14) in terms of Bessel function $J_{np}(\alpha_k r)$ of the first kind and order np [25]:

$$\Phi_i(r,\theta,z,t) = \Re\left\{ \sum_{n=1}^{\infty}\sum_{k=1}^{\infty} \overline{\Phi}_i(z) J_{np}(\alpha_k r) e^{jnp(\theta-\Omega t)} \right\} \tag{15}$$

with

$$\overline{\Phi}_i(z) = \overline{A}_i e^{\alpha_k z} + \overline{B}_i e^{-\alpha_k z} \tag{16}$$

where k is a positive integer (n is an odd positive integer). The values of α_k are determined thanks to the boundary condition $\Phi_i = 0$ for $r = R_3$, which corresponds to the kth zero of the Bessel function of order np:

$$J_{np}(\alpha_k R_3) = 0 \tag{17}$$

The complex coefficients $\overline{A}_i$ and $\overline{B}_i$ in (16) will be determined by using the interface conditions in the z-direction.

Fig. 3 shows the magnetization distribution $M_z(r,\theta,t)$ along the r and θ-direction at $t = 0$ (region 2). The magnetization can be developed into Fourier-Bessel series as follows

$$M_z(r,\theta,t) = \Re\left\{ \sum_{n=1}^{\infty}\sum_{k=1}^{\infty} M_{nk} J_{np}(\alpha_k r) e^{jnp(\theta-\Omega t)} \right\} \tag{18}$$

with

$$M_{nk} = \frac{4p}{\pi R_3^2 J_{np+1}^2(\alpha_k R_3)} \times \int_0^{R_3} \int_{-\pi/2p}^{\pi/2p} M_z(r,\theta) J_{np}(\alpha_k r)\cos(np\theta)\, r dr d\theta \tag{19}$$

From (19) and using the magnetization distribution given in Fig. 3, we obtain

$$M_{nk} = \frac{8B_r}{n\pi\mu_0 R_3^2 J_{np+1}^2(\alpha_k R_3)} \sin\left(n\alpha\frac{\pi}{2}\right) \int_{R_1}^{R_2} r J_{np}(\alpha_k r)\, dr \tag{20}$$

where B_r is the remanent flux density of the magnets and α the pole-arc to pole-pitch ratio of the PMs. Integral in (20) can be determinate numerically or by its analytical expression which is given in the appendix.

From (15), the three components of the magnetic field in each region (i = 1, 2, 3) are given by

$$\mathrm{H}_{ri} = -\frac{\partial \Phi_i}{\partial r} \;;\; \mathrm{H}_{\theta i} = -\frac{1}{r}\frac{\partial \Phi_i}{\partial \theta} \;;\; \mathrm{H}_{zi} = -\frac{\partial \Phi_i}{\partial z} \tag{21}$$

C. Magnetic Field in the Conducting Regions

For the conducting regions (i = 4, 5), the quasi-static Maxwell's equations are used to model the problem

$$\nabla \times \mathbf{H}_i = \mathbf{J}_i \qquad \nabla \cdot \mathbf{B}_i = 0$$
$$\nabla \times \mathbf{E}_i = -\frac{\partial \mathbf{B}_i}{\partial t} \tag{22}$$

where $\mathbf{E}_i$ is the electric field and $\mathbf{J}_i$ the induced current density. As the stationary frame is fixed to the conducting regions, Ohm's law is expressed as

$$\mathbf{J}_i = \sigma_i \mathbf{E}_i \tag{23}$$

where σ_i is the electrical conductivity of region i.

At this point an important question arises: what is the best formulation to solve the problem in the conducting regions as simply as possible? In [14], we have chosen a **H**-formulation to solve a similarly problem but in Cartesian coordinate. Nevertheless, we had to solve two partial differential equations because the magnetic field strength includes three components and $\nabla \cdot \mathbf{H}_i = 0$. We have also shown in [14] that the induced currents in the conducting regions are laminar and flow in the r-θ planes, therefore the current density presents only two components:

$$\mathbf{J}_i = J_{ri}(r,\theta,z,t)\mathbf{e_r} + J_{\theta i}(r,\theta,z,t)\mathbf{e_\theta} \tag{24}$$

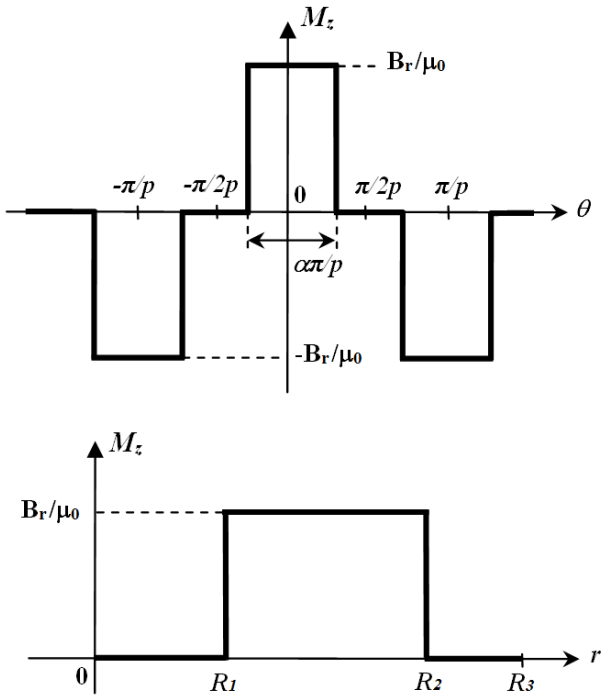

Fig. 3. Magnetization distribution along the r- and θ-direction.

Knowing that $\nabla \cdot \mathbf{J}_i = 0$, it is therefore easier to address this problem by choosing a **J**-formulation. In this way, we have to solve only one partial differential equation that corresponds to one component of the current density.

Manipulating (22) and (23) gives the following diffusion equation for the induced current density

$$\nabla^2 \mathbf{J}_i = \sigma_i \mu_i \frac{\partial \mathbf{J}_i}{\partial t} \tag{25}$$

where μ_i is the permeability of region i. Written in cylindrical coordinates and considering (24), (25) can be split into two coupled partial differential equations

$$\frac{\partial^2 J_{ri}}{\partial r^2} + \frac{1}{r}\frac{\partial J_{ri}}{\partial r} + \frac{1}{r^2}\frac{\partial^2 J_{ri}}{\partial \theta^2} + \frac{\partial^2 J_{ri}}{\partial z^2} - \frac{2}{r^2}\frac{\partial J_{\theta i}}{\partial \theta} - \frac{J_{ri}}{r^2} = \sigma_i \mu_i \frac{\partial J_{ri}}{\partial t} \tag{26}$$

$$\frac{\partial^2 J_{\theta i}}{\partial r^2} + \frac{1}{r}\frac{\partial J_{\theta i}}{\partial r} + \frac{1}{r^2}\frac{\partial^2 J_{\theta i}}{\partial \theta^2} + \frac{\partial^2 J_{\theta i}}{\partial z^2} + \frac{2}{r^2}\frac{\partial J_{ri}}{\partial r} - \frac{J_{\theta i}}{r^2} = \sigma_i \mu_i \frac{\partial J_{\theta i}}{\partial t} \tag{27}$$

As $\nabla \cdot \mathbf{J}_i = 0$, we obtain the following relation between J_{ri} and $J_{\theta i}$

$$\frac{\partial (r J_{ri})}{\partial r} + \frac{\partial J_{\theta i}}{\partial \theta} = 0 \tag{28}$$

Using (26) and (28), and defining a new function $X_{ri} = rJ_{ri}$, we obtain a simpler and decoupled partial differential equation which is directly linked to the r-component of the induced current density

$$\frac{\partial^2 X_{ri}}{\partial r^2}+\frac{1}{r}\frac{\partial X_{ri}}{\partial r}+\frac{1}{r^2}\frac{\partial^2 X_{ri}}{\partial \theta^2}+\frac{\partial^2 X_{ri}}{\partial z^2}=\sigma_i\mu_i\frac{\partial X_{ri}}{\partial t} \tag{29}$$

The boundary conditions given by (4)-(6) can be re-written in terms of the new function X_{ri} as follows

$$\begin{aligned} &X_{ri}(r,-\pi/2p,z,t)=-X_{ri}(r,\pi/2p,z,t)\\ &X_{ri}(R_3,\theta,z,t)=0\\ &X_{ri}(r,\theta,z,t) \text{ is finite at } r = 0 \end{aligned} \tag{30}$$

Finally, we have the same boundary value problem to solve as the one given by (13) and (14), apart from the second member in (29), but this is not a problem because the solution is time-harmonic as indicated by (3). Using the method of separation of variables, general solution of (29) which satisfies the boundary conditions (30) is given by

$$X_{ri}(r,\theta,z,t)=\Re\left\{\sum_{n=1}^{\infty}\sum_{k=1}^{\infty}\overline{X}_{ri}(z)J_{np}(\alpha_k r)e^{jnp(\theta-\Omega t)}\right\} \tag{31}$$

with

$$\overline{X}_{ri}(z)=\overline{A}_i e^{\gamma_k z}+\overline{B}_i e^{-\gamma_k z} \tag{32}$$

and

$$\gamma_k=\sqrt{\alpha_k^2+jnp\sigma_i\mu_i\Omega} \tag{33}$$

where α_k is obtained from (17). The radial and circumferential components of the induced currents are respectively obtained from $J_{ri}=X_{ri}/r$ and (28), and are given by

$$J_{ri}(r,\theta,z,t)=\Re\left\{\sum_{n=1}^{\infty}\sum_{k=1}^{\infty}\overline{X}_{ri}(z)\frac{1}{r}J_{np}(\alpha_k r)e^{jnp(\theta-\Omega t)}\right\} \tag{34}$$

$$J_{\theta i}(r,\theta,z,t)=\Re\left\{\sum_{n=1}^{\infty}\sum_{k=1}^{\infty}j\frac{1}{np}\overline{X}_{ri}(z)J'_{np}(\alpha_k r)e^{jnp(\theta-\Omega t)}\right\} \tag{35}$$

where J'_{np} is the derivative of J_{np} given by

$$J'_{np}(\alpha_k r)=\alpha_k J_{np-1}(\alpha_k r)-\frac{np}{r}J_{np}(\alpha_k r) \tag{36}$$

The complex coefficients $\overline{A}_i$ and $\overline{B}_i$ in (32) will be determined in the next section by using the interface conditions in the *z*-direction.

D. Unknown Coefficients Determination

Equations (16) and (32) show that we have two unknown coefficients to determine for each region. Because we have five regions for this problem (Fig. 2), this means that we need ten independent linear equations. The first two equations are obtained by considering the boundary condition (7) and (8) which can be re-written in terms of magnetic scalar potential Φ and the function X_r. Moreover, we know that the normal component of the magnetic flux density and the tangential component of the magnetic field strength are continuous between two regions. These interface conditions give eight independent linear equations including two equations with the source term M_{nk} defined in (20)

$$\text{for } z=0 \qquad \frac{\partial\overline{\Phi}_1}{\partial z}=0 \tag{37}$$

$$\text{for } z=z_1 \qquad \begin{cases}\overline{\Phi}_1=\overline{\Phi}_2\\ \mu_{rb}\dfrac{\partial\overline{\Phi}_1}{\partial z}=\dfrac{\partial\overline{\Phi}_2}{\partial z}+M_{nk}\end{cases} \tag{38}$$

$$\text{for } z=z_2 \qquad \begin{cases}\overline{\Phi}_2=\overline{\Phi}_3\\ \dfrac{\partial\overline{\Phi}_2}{\partial z}=\dfrac{\partial\overline{\Phi}_3}{\partial z}+M_{nk}\end{cases} \tag{39}$$

$$\text{for } z=z_3 \qquad \begin{cases}\overline{\Phi}_3=\dfrac{1}{n^2p^2\sigma_c\mu_0\Omega}\dfrac{\partial\overline{X}_{r4}}{\partial z}\\ \dfrac{\partial\overline{\Phi}_3}{\partial z}=\dfrac{\alpha_k^2}{n^2p^2\sigma_c\mu_0\Omega}\overline{X}_{r4}\end{cases} \tag{40}$$

$$\text{for } z=z_4 \qquad \begin{cases}\overline{X}_{r4}=\dfrac{\sigma_c}{\sigma_b}\overline{X}_{r5}\\ \dfrac{\partial\overline{X}_{r4}}{\partial z}=\dfrac{\sigma_c}{\sigma_b\mu_{rb}}\dfrac{\partial\overline{X}_{r5}}{\partial z}\end{cases} \tag{41}$$

$$\text{for } z=z_5 \qquad \overline{X}_{r5}=0 \tag{42}$$

where σ_c, σ_b, and μ_{rb} are the copper conductivity, the back-iron conductivity, and the back-iron relative permeability, respectively. Using the ten independent linear equations given above, all the unknown constants $\overline{A}_i$ and $\overline{B}_i$ can be obtained. Developments are given in the appendix.

E. Torque Expression

To determine the electromagnetic torque expression, we apply the Maxwell stress tensor method on a circular disc of radius R_3 placed in the air-gap region (region 3)

$$T=\mu_0\int_0^{R_3}\int_0^{2\pi}H_{z3}(r,\theta,z,t)H_{\theta3}(r,\theta,z,t)r^2drd\theta \tag{43}$$

where H_{z3} and $H_{\theta3}$ can be derived from (15) and (21). From (43), we can express the torque as a function of the unknown coefficients $\overline{A}_3$ and $\overline{B}_3$ of regions 3

$$T=\frac{\pi}{2}\mu_0R_3^2p\Re\left\{\sum_{n=1}^{\infty}\sum_{k=1}^{\infty}jn\alpha_k J_{np+1}^2(\alpha_k R_3)\left(\overline{A}_3^*\overline{B}_3-\overline{A}_3\overline{B}_3^*\right)\right\} \tag{44}$$

where $\overline{A}_3^*$ is the complex conjugate of $\overline{A}_3$.

IV. Model Validation

The main objective here is to show the benefit of the 3-D analytical model proposed in this paper compared to the one we have recently presented in [14]. The analytical model in [14] was 3-D but did not take into account the curvature effects. To show the effectiveness of the new analytical model, the results will be compared with 3-D finite-element simulations by using COMSOL Multiphysics® software. The FE simulations (**A**-φ formulation) are carried out on the actual cylindrical coupling shown in Fig. 1. An infinite box surrounds the studied system in order to set boundary conditions. As the back-iron thickness have been chosen to avoid magnetic saturation, we consider a constant value for the relative permeability of the ferromagnetic parts $\mu_{rb} = 1000$. Only 1 pole of the coupler is considered in the FE analysis with anti-periodic boundary conditions in the circumferential direction.

A. Curvature Effects

As shown in [15] and [16], the curvature effects can be analyzed in an effective manner by considering a dimensionless number λ defines as the ratio of the radial excursion of the magnets $\Delta R = R_2 - R_1$ around the mean radius $R_{mean} = (R_1 + R_2)/2$ to the pole pitch τ:

$$\lambda = \frac{\Delta R}{\tau} \quad \text{with} \quad \tau = \frac{\pi}{p} R_{mean} \tag{45}$$

A large value for λ means that the curvature of the magnetic coupling is pronounced. For the analysis, we consider the geometrical parameters given in Table I. The mean radius of the magnets is fixed to R_{mean} = 45mm and ΔR = 40mm. In order to change the value of λ given in (45), the pole pitch value is varied by changing the pole-pairs number from p = 1 to p = 15, which gives $0.28 < \lambda < 4.24$. The other parameters are kept constant and are those given in Table I.

Fig. 4(a) and Fig. 5(a) respectively show the geometrical distribution of the PMs by considering p = 4 and p = 10 which corresponds respectively to λ = 1.13, and λ = 2.83. For these geometries and for an air-gap value c = 5mm, we have computed the torque-slip characteristic with three different models:

- the 3-D FE model which is considered as the reference model,
- the torque formula (39) given in [14] for which the curvature effects was neglected,
- the torque expression (44) given in this paper which considers the curvature effects.

The results given in Fig. 4(b) clearly show that the torque versus slip speed characteristic is well determinate with both 3-D analytical models if the curvature coefficient $\lambda \simeq 1$. When the curvature coefficient increases, this is not longer true and we can observe in Fig. 5(b) that the error on the torque prediction is important by using the 3-D analytical model developed in Cartesian coordinates [14]. On the other hand, the results obtained with the 3-D analytical model developed in this paper (44) which considers the curvature effects remain very accurate.

TABLE I
PARAMETERS OF THE STUDIED EDDY-CURRENT COUPLING

Symbol	Quantity	value
R_1	Inner radius of the magnets	25 mm
R_2	Outer radius of the magnets	65 mm
R_3	Outer radius of the conducting plate	90 mm
a	Thickness of the back-iron (magnets side)	10 mm
b	Magnets thickness	10 mm
c	Air-gap length	variable
d	Copper thickness	5 mm
e	Thickness of the back-iron (copper side)	8 mm
α	PMs pole-arc to pole-pitch ratio	0.9
p	Pole-pairs number	variable
B_r	Remanence of the permanent magnets (NdFeB)	1.25 T
σ_c	Conductivity of the copper	57 MS/m
σ_b	Conductivity of the back-iron	7 MS/m
μ_{rb}	Relative permeability of the back-iron	1000

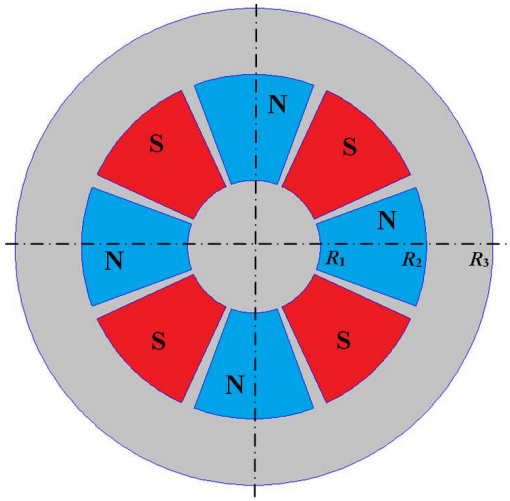

(a)

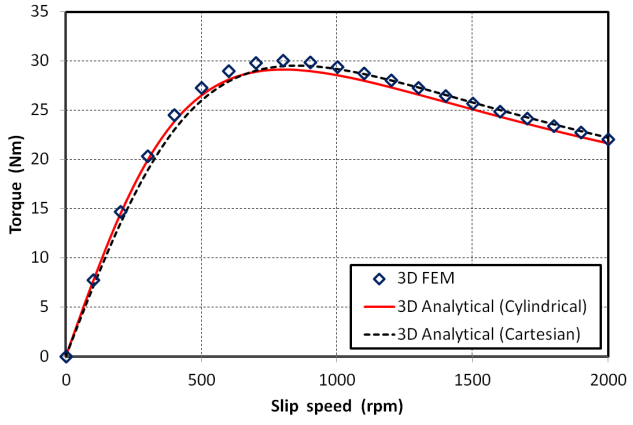

(b)

Fig. 4. PMs distribution (a), and Torque-slip speed characteristic (b) for p = 4 (λ = 1.14) and c = 5mm.

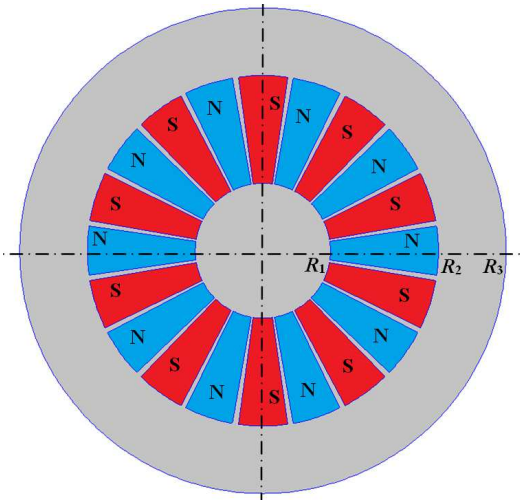

(a)

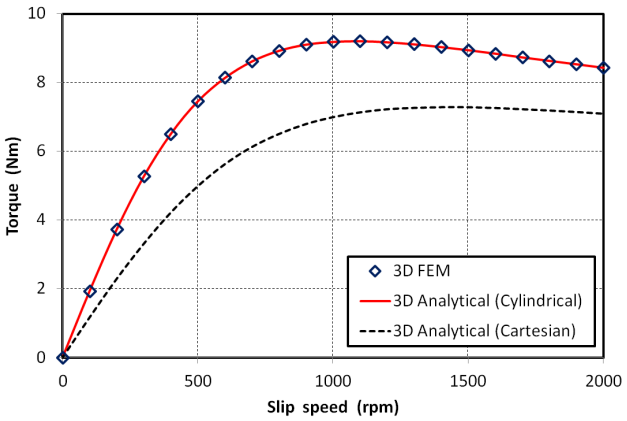

(b)

Fig. 5. PMs distribution (a), and Torque-slip speed characteristic (b) for $p = 10$ ($\lambda = 2.28$) and $c = 5$mm.

Fig. 6 gives the relative error on the torque prediction between the two 3-D analytical models (with or without the curvature effects). The error is defined as follows

$$\varepsilon_{\%} = 100 \times \frac{T_{cylindrical} - T_{cartesian}}{T_{cylindrical}} \qquad (46)$$

where $T_{cylindrical}$ is the torque obtained using (44) and $T_{cartesian}$ is the torque obtained using the formula (39) in [14]. The results given in Fig. 6 have been computed for a slip speed of 300rpm and by considering three values for the air-gap length (1mm, 3mm and 5mm).

It can be noted that the error between the two models remains lower than 5% until the curvature coefficient λ is not greater than about 1.2. When λ increase, the error becomes significant and can be greater than 50% when the curvature effects are very pronounced. These results show the limits of the 'linearized' model [14] to represent a cylindrical structure. Another important point when we compared 3-D analytical models with 3-D FE models is the computation time. This is an important issue if the model has to be used in an optimization procedure.

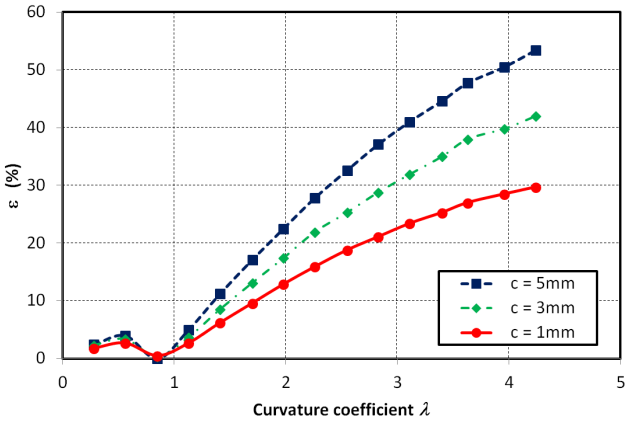

Fig. 6. Error on the torque prediction between 3-D analytical models (Cylindrical and Cartesian) for three values of the air gap length at 300rpm.

The torque-speed characteristics given in Fig. 5(b) have been computed in 0.1s when using 3-D analytical model whereas it takes more than 3 hours with 3-D FE model. Because the Bessel functions converge very rapidly, the number of harmonic terms needed for the analytical model remains very low, the first five harmonics in the r- and θ-directions are sufficient to obtain accurate results.

B. Induced Currents distribution in the copper

Fig. 7 compares the eddy-current density distribution in the copper along the θ-direction at $r = R_2$ obtained with 3-D FEM and with the proposed analytical formulas (34) and (35), for a slip speed of 1000rpm. We can observe that the two components of the induced current are well predicted by the 3-D analytical model in terms of amplitudes and waveforms. Since the number of pole-pairs is large ($p = 10$) and the air-gap length is important ($c = 5$mm), the harmonic components of the induced currents are mitigated and the current distribution shown in Fig. 7 is quasi-sinusoidal.

Fig. 8 shows the eddy-current density distribution in the middle of the copper plate along the r-direction at $\theta = 0$. These results clearly show the ability of the proposed 3-D analytical model to predict the induced currents distribution in the radial direction when the curvature effects are significant. In fact, we can observe in Fig. 8 that the eddy-current density distribution is not symmetrical around the mean radius ($R_{mean} = 45$mm), that would be the case if the linearized model [14] was used, resulting in important errors for the torque prediction as shown in Fig .5(b).

C. Impact of the Conductor Back-Iron on the Torque Value

The 3-D analytical model developed in this paper takes into account the eddy-currents induced in the back-iron (copper side) and their contribution to the torque (44). Indeed, the problem has been solved in region 5 of Fig. 2 and mathematical expressions for the radial and circumferential components of the current density in this region have been obtained (34), (35).

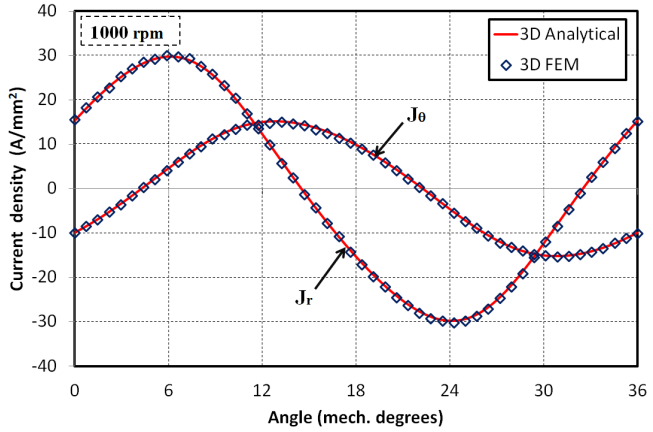

Fig. 7. Eddy-current density distribution along the θ-direction for $r = R_2$, $z = (z_3+z_4)/2$, $p = 10$, $c = 5$mm and 1000rpm.

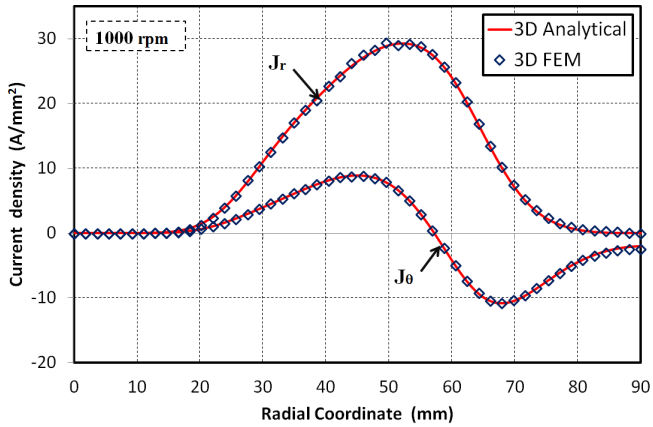

Fig. 8. Eddy-current density distribution along the r-direction for $\theta = 0$, $z = (z_3+z_4)/2$, $p = 10$, $c = 5$mm and 1000rpm.

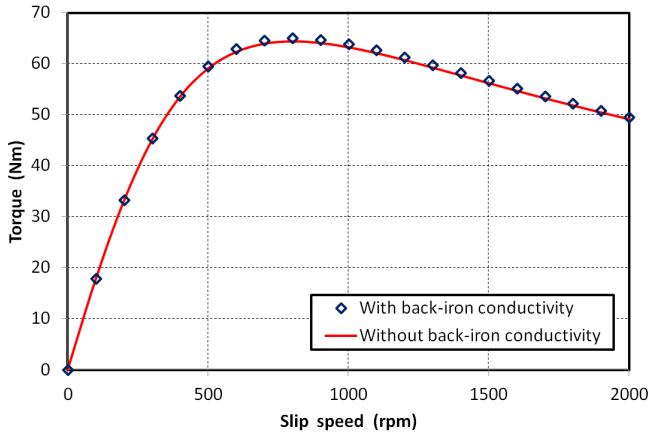

Fig. 9. Back-iron conductivity effect on the torque-slip characteristic for $p = 4$ and $c = 1$mm.

In order to investigate the contribution of the induced currents in the back iron, we compared the torque-slip characteristics obtained by considering the back-iron conductivity (σ_b = 7MS/m) and by ignoring it (σ_b = 0MS/m). We consider the geometrical parameters given in Table I with $p = 4$ and $c = 1$mm. The results are given in Fig. 9. It can be observed that the eddy-currents induced in the back-iron have a negligible influence on the torque. The difference between the two characteristics is never greater than 2%. This result has been confirmed with other geometrical values and is in accordance with the results given in [6] and [7]. Therefore, it is possible to neglect the back-iron conductivity in order to obtain a simpler model for the axial-field eddy-current magnetic coupling, as it is illustrated in the next section.

D. Simplified Model and Closed-Form Expression for the Torque

It has been shown in the previous section that the eddy currents induced in the back-iron have a negligible influence on the torque value and can be neglected in the model. Moreover, the back-iron thicknesses a and e in Fig. 1 have to be designed to avoid magnetic saturation. Therefore, to simplify the model we consider an infinite permeability for regions 1 and 5 of Fig. 2. The whole domain of the field problem is then reduced to only three regions (regions 2, 3 and 4 of Fig. 2) with the following boundary conditions which are directly related to the infinite permeability assumption for regions 1 and 5:

$$\mathbf{H}_2 \times \mathbf{e}_z = 0 \quad \text{at} \quad z = z_1 \tag{47}$$

$$\mathbf{H}_4 \times \mathbf{e}_z = 0 \quad \text{at} \quad z = z_4 \tag{48}$$

With the previous assumptions, it is now possible to obtain a closed-form expression for the torque. After some rather long calculations to determine the expressions of all unknown coefficients and particularly those of region 3 which appear directly in the torque expression (44), we obtain the following torque formula that depends directly on the physical and geometrical parameters and can be used as it is:

$$T = \frac{\pi}{2}\mu_0 R_3^2 p \Re\left\{\sum_{n=1}^{N}\sum_{k=1}^{K} jn \frac{M_{nk}^2}{\alpha_k} J_{np+1}^2(\alpha_k R_3)\,\bar{r}\sinh(\alpha_k b)\right\} \tag{49}$$

with

$$\bar{r} = \frac{\sinh(\alpha_k c)\cosh(\gamma_k d) + \frac{\gamma_k}{\alpha_k}\cosh(\alpha_k c)\sinh(\gamma_k d)}{\sinh(\alpha_k (b+c))\cosh(\gamma_k d) + \frac{\gamma_k}{\alpha_k}\cosh(\alpha_k (b+c))\sinh(\gamma_k d)}$$

where $\Re$ denotes the real part of a complex number, $j = \sqrt{-1}$, M_{nk} is given by (20), α_k and γ_k are respectively given by (17) and (33), J_{np+1} is the Bessel function of the first kind and order $np+1$, n is an odd integer and k is an integer.

Using (49), the torque-slip characteristic given in Fig. 9 is obtained in a few tens of milliseconds whereas it needs more than one hour with the 3-D FE model with the same assumptions.

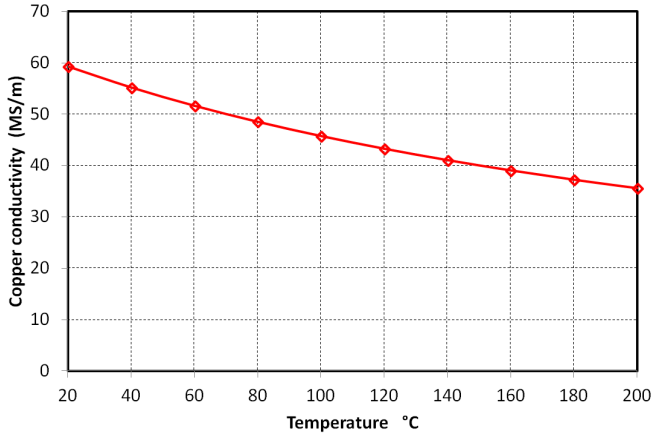

Fig. 10. Conductivity of copper as a function of the temperature.

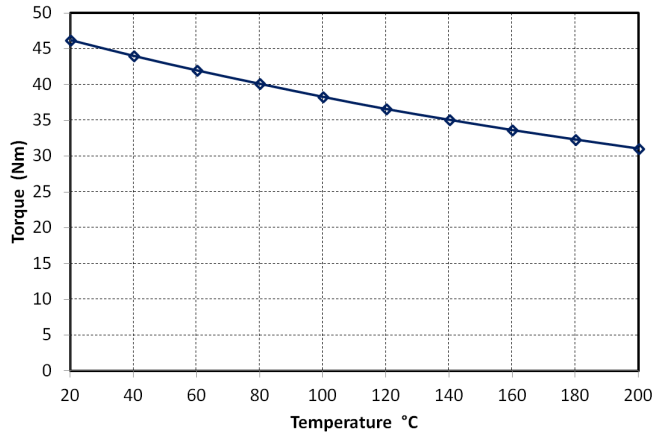

Fig. 11. Torque versus temperature for $p = 4$, $c = 1$mm and 300rpm.

E. Effect of the Temperature on the Torque value

In this paper, we have considered a constant value for the copper conductivity. However, it is well-known that due to the eddy-current losses, the temperature of the copper will rise, and even more as the slip speed is important. As the electrical conductivity of the copper decreases with the temperature, this will have a direct impact on the torque-slip speed characteristic. Therefore, a complete design of eddy-current magnetic couplings requires both magnetic and thermal analysis because the magnetic and thermal fields are coupled each other. A thermal analysis based on thermal network model has been recently proposed in [23] and has given accurate results. Fig.10 shows the variation of the copper conductivity as a function of the temperature. This has a direct impact on the torque value (49) as can be seen in Fig. 11. A temperature of 200°C, classically reached in braking operation, can cause a 31% drop on the torque value in comparison with the ambient temperature.

V. Conclusion

In this paper, a novel 3-D analytical model has been proposed for the analysis of axial-field eddy-current magnetic couplings. The analytical model has been obtained by solving the Maxwell equations in a 3-D cylindrical coordinate system. Compared to previous analytical models available in the literature, the proposed model directly takes into account the radial edge effects and the curvature effects without the need of using correction factors as it is usually done. Comparisons with 3-D FE simulations have shown that the proposed analytical model is very accurate to predict the torque-slip characteristic, even for the geometries where the curvature effects are very pronounced. On this point, we have shown the limits of the approximated 3-D analytical models using the mean radius development assumption.

As the proposed model is very efficient in terms of precision and computation time, it can be effectively used in a design optimization procedure where the geometrical parameters can vary significantly.

Appendix

● From (37) to (42), we obtain a system of ten equations with ten unknown complex coefficients:

$$
\begin{aligned}
&\overline{A}_1 - \overline{B}_1 = 0\\
&\overline{A}_1 e^{\alpha_k z_1} + \overline{B}_1 e^{-\alpha_k z_1} = \overline{A}_2 e^{\alpha_k z_1} + \overline{B}_2 e^{-\alpha_k z_1}\\
&\overline{A}_1 e^{\alpha_k z_1} - \overline{B}_1 e^{-\alpha_k z_1} = \frac{1}{\mu_{rb}}\left(\overline{A}_2 e^{\alpha_k z_1} + \overline{B}_2 e^{-\alpha_k z_1} + \frac{M_{nk}}{\alpha_k}\right)\\
&\overline{A}_2 e^{\alpha_k z_2} + \overline{B}_2 e^{-\alpha_k z_2} = \overline{A}_3 e^{\alpha_k z_2} + \overline{B}_3 e^{-\alpha_k z_2}\\
&\overline{A}_2 e^{\alpha_k z_2} - \overline{B}_2 e^{-\alpha_k z_2} = \overline{A}_3 e^{\alpha_k z_2} - \overline{B}_3 e^{-\alpha_k z_2} + \frac{M_{nk}}{\alpha_k}\\
&\overline{A}_3 e^{\alpha_k z_3} + \overline{B}_3 e^{-\alpha_k z_3} = \frac{\lambda_k}{n^2 p^2 \sigma_c \mu_0 \Omega}\left(\overline{A}_4 e^{\lambda_k z_3} - \overline{B}_4 e^{-\lambda_k z_3}\right)\\
&\overline{A}_3 e^{\alpha_k z_3} - \overline{B}_3 e^{-\alpha_k z_3} = \frac{\alpha_k}{n^2 p^2 \sigma_c \mu_0 \Omega}\left(\overline{A}_4 e^{\lambda_k z_3} + \overline{B}_4 e^{-\lambda_k z_3}\right)\\
&\overline{A}_4 e^{\lambda_k z_4} + \overline{B}_4 e^{-\lambda_k z_4} = \frac{\sigma_c}{\sigma_b}\left(\overline{A}_5 e^{\lambda_k z_4} + \overline{B}_5 e^{-\lambda_k z_4}\right)\\
&\overline{A}_4 e^{\lambda_k z_4} - \overline{B}_4 e^{-\lambda_k z_4} = \frac{\sigma_c}{\mu_{rb}\sigma_b}\left(\overline{A}_5 e^{\lambda_k z_4} - \overline{B}_5 e^{-\lambda_k z_4}\right)\\
&\overline{A}_5 e^{\lambda_k z_5} + \overline{B}_5 e^{-\lambda_k z_5} = 0
\end{aligned}
\tag{A.1}
$$

The ten unknown coefficients in (A.1) can be determined numerically by solving the linear system of equations (A.1) using mathematical software (Matlab or Maple).

● The magnetization distribution (20) depends on the following integral issued from the orthogonal properties of the Bessel function

$$I = \int_{R_1}^{R_2} r J_{np}(\alpha_k r)\, dr \tag{A.2}$$

This integral can be computed numerically or by its analytical expression

$$\int xJ_n(ax)\,dx = 2^{-(1+n)}x^2(ax)^n \frac{\Gamma\left(1+\frac{n}{2}\right)}{\Gamma(1+n)\Gamma\left(2+\frac{n}{2}\right)} \times \mathrm{F}\left(1+\frac{n}{2};\left[1+n,2+\frac{n}{2}\right];-\frac{1}{4}a^2x^2\right) \quad \text{(A.3)}$$

where Γ is the Gamma function and F the Hypergeometric function [25].

REFERENCES

[1] E. J. Davies, "An experimental and theoretical study of eddy-current couplings and brakes," *IEEE Trans. Power App. Syst.*, vol. 82, no. 67, pp. 401-419, Aug. 1963.

[2] A. Canova, and B. Vusini, "Design of axial eddy-current couplers," *IEEE Trans. Ind. Appl.*, vol. 39, no. 3, pp. 1725–1733, May/June 2003.

[3] A. Canova, and B. Vusini, "Analytical modeling of rotating eddy-current couplers," *IEEE Trans. Magn.,* vol. 41, no. 1, pp. 24-35, Jan. 2005.

[4] H. J. Shin, J. Y. Choi, H. W. Cho, and S. M. Jang, "Analytical torque calculation and experimental testing of permanent magnet axial eddy current brake," *IEEE Trans. Magn.*, vol. 49, no. 7, pp. 4152–4155, Jul. 2013.

[5] J. Wang, H. Lin, S. Fang, and Y. Huang, "A general analytical model of permanent magnet eddy current couplings," *IEEE Trans. Magn.*, vol. 50, no. 1, p. 8 000 109, Jan. 2014.

[6] X. Dai, Q. Liang, J. Cao, Y. Long, J. Mo, and S. Wang, "Analytical modelling of axial-flux permanent magnet eddy current couplings with slotted conductor topology," *IEEE Trans. Magn.*, vol. 52, no. 2, p. 8 000 315, Feb. 2016.

[7] J. Wang, H. Lin, and S. Fang, "Analytical prediction of torque characteristics of eddy current coupling having a quasi-Halbach magnet structure," *IEEE Trans. Magn.*, vol. 52, no. 6, p. 8 001 209, Jun. 2016.

[8] R. Yazdanpanah, and M. Mirsalim, "Axial-flux wound-excitation eddy-current brakes: analytical study and parametric modeling," *IEEE Trans. Magn.*, vol. 50, no. 6, p. 8000710, Jun. 2014..

[9] S. Mohammadi, M. Mirsalim, and S. Vaez-Zadeh, "Non-linear modeling of eddy-current couplers," *IEEE Trans. Energy Convers.*, vol. 29, no. 1, pp. 224–231, Mar. 2014.

[10] Z. Mouton, and M. J. Kamper, "Modeling and Optimal Design of an Eddy Current Coupling for Slip-Synchronous Permanent Magnet Wind Generators," *IEEE Trans. Ind. Electron.*, vol. 61, no. 7, pp. 3367–3376, Jul. 2014.

[11] R. L. Russell and K. H. Norsworthy, "Eddy currents and wall losses in screened-rotor induction motors," *Proc. Inst. Elect. Eng*., vol. 105, no. 20, pp. 163- 175, Apr. 1958.

[12] M. G. Malti and R. Ramakumar, "Three-dimensional theory or the eddy-current coupling," *IEEE Trans. Power App. Syst.*, vol. 82, no. 68, pp. 793–800, Oct. 1963.

[13] E. J. Davies, M. T. Wright, and H. Mckibbin, "Three-dimensional theory of eddy-current couplings with copper-faced loss drums," *Proc. Inst. Electr. Eng*., vol. 124, no. 12, pp. 1187–1196, Dec. 1977.

[14] T. Lubin and A. Rezzoug, "3-D analytical model for axial-flux eddy current couplings and brakes under steady-state conditions," *IEEE Trans. Magn.*, vol. 51, no. 10, p. 820371, Oct. 2015.

[15] O. de la Barrière, S. Hlioui, H. Ben-Ahmed, M. Gabsi, and M. LoBue, "3-D formal resolution of Maxwell equations for the computation of the no-load flux in an axial flux permanent-magnet synchronous machine," *IEEE Trans. Magn*., vol. 48, no. 1, pp. 128–136, Jan. 2012.

[16] B. Dolisy, S. Mezani, T. Lubin, and J. Lévêque, "A new analytical torque formula for axial field permanent magnets coupling," *IEEE Trans. Energy Convers.*, vol. 30, no. 3, pp. 892-899, Sep. 2015.

[17] K. R. Shao, and J. D. Lavers, "Method of fundamental solutions based on the second order vector potential formulation for 3D eddy current analysis," *IEEE Trans. Magn.,* vol.29, no.6, pp. 2431-2433, Nov. 1993.

[18] F. Henrotte, H. Heumann, E. Lange, and K. Hameyer, "Upwind 3-D vector potential formulation for electromagnetic braking simulations," *IEEE Trans. Magn*., vol. 46, no. 8, pp. 2835–2838,Aug. 2010.

[19] J. Bird, and T. A. Lipo, "Modeling the 3-D rotational and translational motion of a Halbach rotor above a split-sheet guideway," *IEEE Trans. Magn.*, vol. 45, no. 9, pp. 3233–3242, Sep. 2009.

[20] S. Paul, W. Bomela, N. Paudel, and J. Z. Bird, "3-D eddy-current torque modeling," *IEEE Trans. Magn.,* vol.50, no.2, p. 7022404, Feb. 2014.

[21] A. C. Smith, S. Williamson, A. Benhama, L. Counter, and J. M. Papadopoulos, "Magnetic drive couplings," in *Proc. IEE 9th EMD,* Canterbury, U.K., Sep. 1-3, 1999, pp. 232-236.

[22] E. J. Davies, "An experimental and theoretical study of eddy-current couplings and brakes," *IEEE Trans. Power App. Syst.*, vol. 82, no. 67, pp. 401-419, Aug. 1963.

[23] D. Zheng, D. Wang, S. Li, T. Shi, Z. Li, and L. Yu, "Eddy current loss calculation and thermal analysis of axial-flux permanent magnet couplers," AIP Advances **7**, 025117, 2017.

[24] T. Lubin, and A. Rezzoug, "Steady-state and transient performance of axial-field eddy-current coupling," *IEEE Trans. Ind. Electron.*, vol. 62, no. 4, pp. 2287–2296, Apr. 2015.

[25] M. Abramowitz, and I. A. Stegun, *Handbook of mathematical functions*, Dover publications, Inc., New York, 1972.